

Analysis of a capped carbon nanotube (CNT) with linear-scaling density-functional theory

ERRATA: 1) The previous version of this paper suggested a relation between potential profile at a surface and image potential that is not consistent with the standard interpretation of DFT. **Some simple edits have been made to correct erroneous statements;** 2) In this type of DFT calculation, the HOMO is not an exact guide to the Fermi level and estimates of the Fermi level are likely to differ substantially from experimental values; 3) in the plots of Fig. 8, the zeros of potential may vary with applied field. Plots with aligned Fermi levels are preferable. A revised version of this paper is in preparation. Meanwhile, the results of computation shown here in the other figures remain valid.

C J Edgcombe*, J Whaley-Baldwin and S M Masur

TFM Group, Department of Physics, University of Cambridge, CB3 0HE, Cambridge, UK

*corresponding author, email cje1@cam.ac.uk

Abstract

The apex region of a capped (5,5) carbon nanotube (CNT) has been analysed by use of the DFT package ONETEP, using boundary conditions provided by a classical calculation with a conducting surface in place of the CNT. Application of an external electric field produces very little change in the charge distribution on the CNT, implying that the potential profile from atom cores to the screening distance also changes little ~~and so is a suitable replacement for the analytic image potential used hitherto.~~ The DFT solution also provides details of the individual orbitals for the CNT tip, their physical distribution and their occupation, ~~allowing the work function to be estimated.~~

Keywords

Carbon nanotube, density functional theory, Wannier functions, charge density, density of states, Fermi level, HOMO

1. Introduction

The challenge of describing field-emitting structures and field emission continues to be addressed by development of methods of analysis. All these methods preserve the concept of tunnelling through a classically-forbidden region that provided one of the first successes of wave mechanics [1]. Yet many further details of the emission process have proved difficult to describe simply, while verification of practical parameters such as the emitting area remains a challenge for experimental technique. Recent developments in microscopy, such as near-field scanning electron microscopy [2], have increased the need for methods that can describe the distribution of emitted current in detail. Some aspects of the conventional semi-analytic theory are unsatisfying, in particular the use of an image potential. While this provides a potential distribution near the surface whose shape ~~must~~ may be qualitatively correct, the standard form implies that the image potential is proportional to the current drawn. It also uses the concept of a continuous conducting surface, which may seem reasonable as a macroscopic concept but at atomic scale ~~has to~~ should be replaced by a structure of atom cores and electrons. Fortunately, a description from first principles can be provided by density functional theory, solved over a limited volume (the ‘DFT box’). This is still not easy to apply to typical field emitters, yet progress has been reported. Zheng et al [3] divided the length of a single-walled CNT (SWCNT) into subranges, iterating by solving each subrange in turn while the others were simulated by molecular mechanics. Csányi et al [4] introduced two new steps: the use of non-planar basis functions for DFT (as outlined below) and use of a classical equivalent to provide the

exterior boundary conditions for the DFT box. Li [5] applied multi-scale DFT to model edges of graphene and open-ended CNTs, and extended the method to calculate emitted current.

Here we describe more details and results from the DFT method used by Csányi et al. The results show that there is a ‘screening’ region between the CNT cores and the maximum of potential in the barrier region. The initial motivation was that the use of plane waves as basis functions, as found in many DFT packages, is unsuitable for non-periodic systems of hundreds of atoms or more. The number of plane waves and the solution time needed to model the system accurately would both be prohibitively large. Instead, we use the package ONETEP (Order-N Electronic Total Energy Package) [6] which works with a basis of localized, adaptable functions that are organized so that the solution time scales only as the number of atoms in the model. The boundary conditions can be specified by the potential distribution over the surface of the DFT box, together with the charge induced into it. The results available include information on individual orbitals, with their spatial distribution and occupation, at a given non-zero temperature. In this paper we report some initial calculations on a SWCNT with a hemispherically capped end.

2. Method of calculation

To obtain a solution within acceptable computing time, we define a limited volume (the ‘DFT box’) over which the density functional calculation will be solved. The volume used in the present work was a cube of side 5 nanometres. Within this volume, the required atomic structure must be defined approximately and allowed to relax to equilibrium. Using the program Virtual Nanolab [7], we built a single-walled cylindrical (5,5) tube of carbon atoms, one end of which was capped with

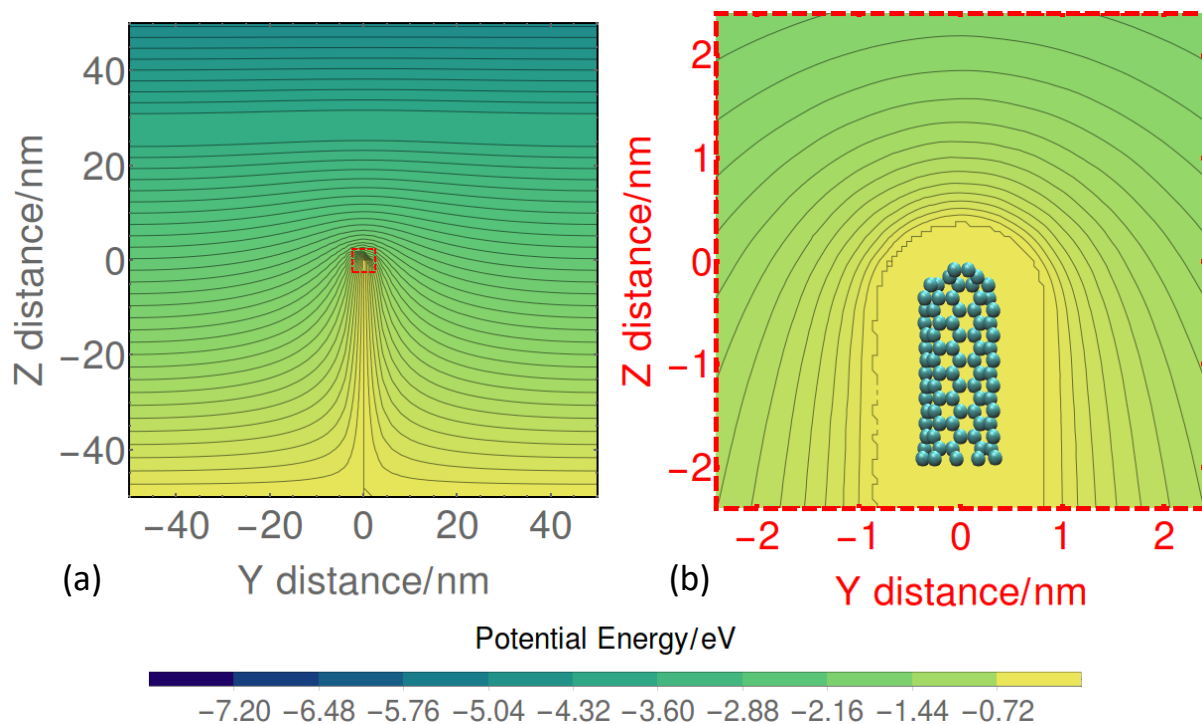


Fig. 1. Geometry analysed: (a) CNT supported on planar cathode electrode at $z = -50$ nm, with parallel anode plane at $z = +50$ nm. The small red box around the CNT tip defines the volume shown in (b); (b) the final 1.8 nm of the capped (cylindrical) CNT, in the (cubic) DFT box of side 5 nm. The potential values shown are for an anode-cathode voltage of 8 V with contours at intervals of 0.2 eV.

half a C_{60} molecule (having a pentagon on its axis). The combination of tube and hemisphere contained 150 carbon atoms and was terminated at the uncapped end with 10 hydrogen atoms. The atomic positions were optimised until the force on each atom was less than 0.05 eV/Å. The optimised CNT has carbon cores at a radius of 0.317 nm from the axis and is 1.83 nm long (Fig. 1(b)). Density functional theory determines the state of a system by minimising a sum of energy terms of the form

$$E[n] = \sum_i \langle \psi_i | -\frac{1}{2} \nabla^2 | \psi_i \rangle + E_{ext}[n] + E_{Coul}[n] + E_{xc}[n]$$

where the first term on the right represents the kinetic energy of a non-interacting system, the second term is the energy due to the externally applied field, the third term is the energy due to classical Coulomb repulsion and the fourth term contains all non-classical effects. The ψ_i are single-particle orbitals and the density $n(\mathbf{r})$ is the sum of the squared moduli of the occupied ψ_i . In many DFT packages, basis sets of the ψ_i are formed from linear combinations of simple functions such as plane waves or Gaussians. However, these bases are not well suited to non-periodic structures and the number of plane waves needed for an adequate representation of the CNT would be prohibitively large. In the program ONETEP [6], $n(\mathbf{r})$ is defined as a sum of quadratic terms, obtained from a kernel matrix and Wannier functions $\phi_\alpha(\mathbf{r})$. The Wannier functions are themselves linear combinations of simpler functions, whose ranges can be controlled. In the DFT solution, both the kernel coefficients and the Wannier functions are varied adaptively. As a result, the solution time scales linearly with the number of orbitals N . For problems with N of the order of hundreds, this property offers a great advantage over other methods whose solution time is proportional to N^3 or more.

The quantities that can be reported on a regular mesh by ONETEP include charge density, potential energy, density of states (DoS), and the energy, occupation and physical distribution of individual states, from which the Fermi level is readily obtained. Calculations are made for a given non-zero temperature. It was found in 2005 [4] with an earlier version of ONETEP that solutions can be obtained for a given potential distribution on the boundary with a given excess electronic charge. The result describes an equilibrium ground state and is usable for external fields below the emission threshold. Even without modelling field-emitted current, the results to be described show much more detail of behaviour than is available from classical approximations and assumptions. A particular benefit is that the program shows the energy and physical distribution of the highest occupied molecular orbital (HOMO) which is of interest as the most likely source of current when emission occurs.

To solve the system with an applied electric field, we use a combination of classical and DFT calculations. The CNT is assumed to conduct sufficiently well that the potential around it is the same as that around a conducting rod of the same dimensions (provided that the classical surface corresponds to an equipotential of the atomic system, as discussed below). For our calculation, the CNT of total length 50.3 nm is assumed to stand perpendicular to and in contact with a cathode plane of diameter 100 nm (Fig. 1(a)). The CNT faces an anode plane of diameter 100nm which is parallel to the cathode plane and spaced from it by 100 nm. With a given voltage between anode and cathode planes, a solution of Laplace's equation for the voltage distribution is obtained using a classical solver such as FlexPDE [8]. The distributions of voltage and normal electric field over the surface of the DFT box are extracted from this solution. The electric field induces charge on the CNT, with the greatest density at the apex. The integral of the normal electric field over the whole surface of the DFT box gives (by Gauss' law) the magnitude of charge induced within the volume of

the box. In this classical model, the CNT is in contact with the cathode plane and the magnitude of the charge induced within the DFT box is a fixed multiple of the anode-cathode voltage.

The known potential distribution over the surface of the box and the charge induced within it can now be supplied as fixed values to the DFT calculation, in which the short section of the CNT as defined above is not connected to the boundary. The DFT conditions then have an extra degree of freedom which allows the added charge to be specified independently of the boundary potential. Variation of this charge would vary the mean potential of the CNT section, relative to the boundary.

3. Results for capped (5,5) SWCNT

3.1 Classical solution

The classical solution was calculated using a conducting cylindrical rod of diameter 0.864 nm, shaped at one end like the CNT and with cathode and anode planes as above, in a rectangular mesh. The resulting equipotentials for this system are shown in Fig. 1(a). Fig. 1(b) shows a section through the volume to be used for the DFT box, with classical equipotentials and the equilibrium structure of the carbon cores superimposed.

3.2 DFT solution without field

The electron density distribution with zero applied field is shown in Fig. 2. Isosurfaces are drawn for densities of 0.12, 1.5 and 6 e/Å³, that is for 0.02%, 0.25% and 1% of the global maximum density (found with zero field as 605 e/Å³). It can be seen immediately that most of the charge is localised near the carbon cores, but there is also a continuous sheath of relatively low density at a slightly greater distance from the cores.

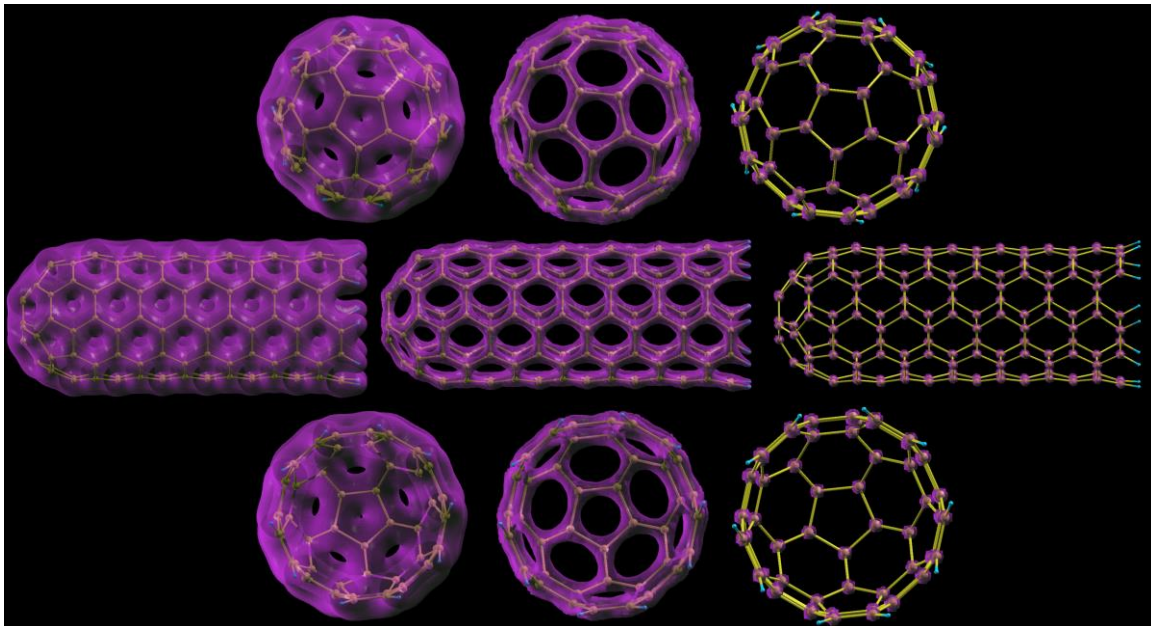


Fig. 2. Electron density isosurfaces for zero applied field (those with '8V' applied field are identical in appearance at this scale). Isosurfaces are in purple with the (yellow) frame of the CNT visible underneath. From left to right, the isosurfaces are at 0.02%, 0.25%, 1.00% of the global maximum charge density ($\approx 0.12, 1.5, 6.0 \text{ e}\text{\AA}^{-3}$ respectively). Top row: View along z-axis from cap. Middle row: Side view. Bottom row: View along z-axis from cap end.

The density of states (DoS) can be found for few or many carbon sites. As a simple example, the CNT has been divided into an end region, containing the four rings of C cores on an approximate

hemisphere, and a body region, containing the remaining cores on the cylinder. Fig. 3 shows, for zero applied field, the local DoS in the two regions, normalized by the number of atoms in each region. The individual peaks have been broadened by Gaussians of width 0.2 eV. Near the Fermi level, there are states in the end cap that are absent from the body.

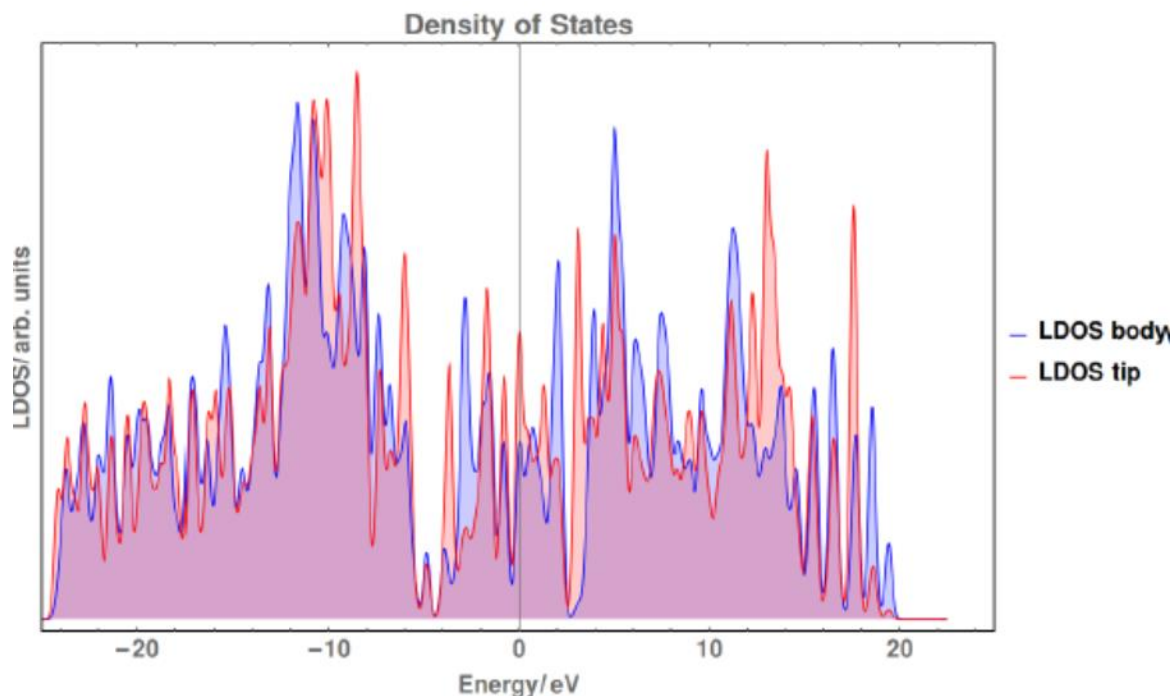


Fig. 3. Normalized local densities of states for tip and body regions of the CNT. The zero of energy is the vacuum level.

ONETEP can report the energy and probability of occupation of individual orbitals. An example is given in Table 1, for a temperature of 1000 K.

Orbital	Energy /Hartree	Occupancy
310	-0.121850780	0.000002700
309	-0.134607169	0.000147200
308	-0.134664059	0.000149900
307	-0.144225281	0.003097400
306	-0.146746421	0.006863900
305	-0.178987464	0.994560200
304	-0.179371931	0.995181300
303	-0.203222517	0.999997400

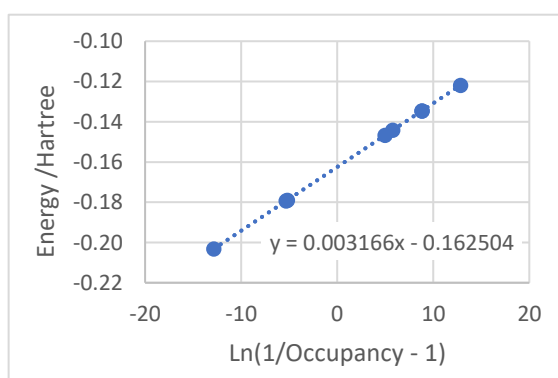


Fig. 4. Plot to test Fermi-Dirac distribution.

A plot of Orbital Energy against $\ln(1/\text{Occupancy} - 1)$, as in Fig. 4, shows good agreement with the Fermi-Dirac distribution, from which [a DFT estimate of the](#) Fermi level E_F can be obtained as -4.422

eV relative to vacuum level. At lower temperatures, the transition in occupation is more abrupt and it is less feasible to extract E_F graphically with the number of atoms used here. The mid-gap value of energy at the transition is found to be $-4.432 \text{ eV} \pm 4 \times 10^{-6} \text{ eV}$ for temperatures of 100, 300 and 1000 K.

Fig. 5 shows an isosurface of the amplitude of the HOMO found for the DFT box. The HOMO appears to have appreciable amplitude at the point where the axis meets the cap, in contrast to the total charge density which according to Fig. 2 is small on the axis. However, this HOMO amplitude is largest on the inside of the frame of carbons so the applied field reaching the HOMO may be attenuated relative to the field outside the frame.

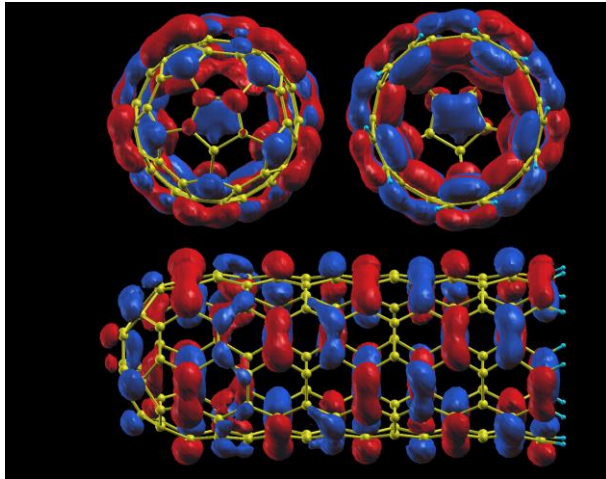


Fig. 5. Isosurface at $\pm 0.015 \text{ (e\AA}^{-3})^{1/2}$ of HOMO for the 5x5 CNT, with zero applied field. Blue regions are positive, red regions are negative.

3.3 DFT solution with applied field

The change in distribution of charge density with applied field is shown in Fig. 6. The magnitude of this change in density shown by the blue isosurface is $5.5 \times 10^{-3} \text{ e/\AA}^3$, which is about 0.3% of the static charge density of the middle surface in Fig. 2. The significance of this small change is discussed below. This was found for an applied field estimated to be about a quarter of that needed to emit current. For this applied field, 2 electrons were supplied to the DFT calculation as induced charge. The relative change of charge density found is approximately consistent with the induction of this charge into the system containing 610 electrons.

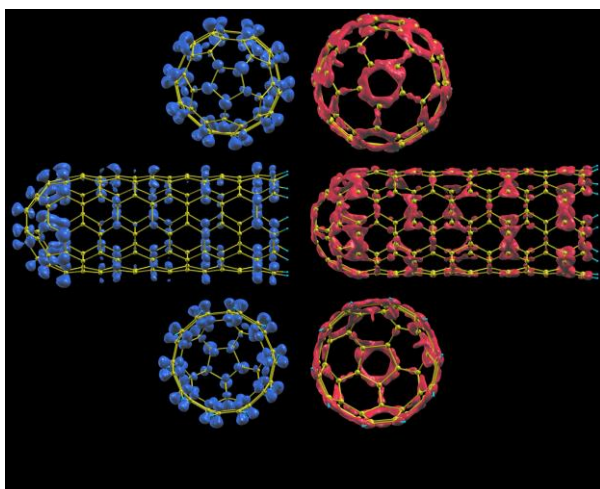


Fig. 6. Change in electron density on application of the '8V' field. The blue isosurface shows where the electron density has increased by $5.5 \times 10^{-3} \text{ e\AA}^{-3}$. The red isosurface shows regions that have decreased by $2.5 \times 10^{-3} \text{ e\AA}^{-3}$.

A longitudinal section through the DFT box, with equipotentials resulting from an applied anode-cathode voltage of 8V, is shown in Fig. 7. The distribution of potential near the hemispherical cap

and cylindrical surface is much smoother than that of charge density, which is reasonable since the potential is a double integral of the charge density, in accordance with Poisson's equation. With the relatively low values of field used, no indication has been seen of field penetration at the apex.

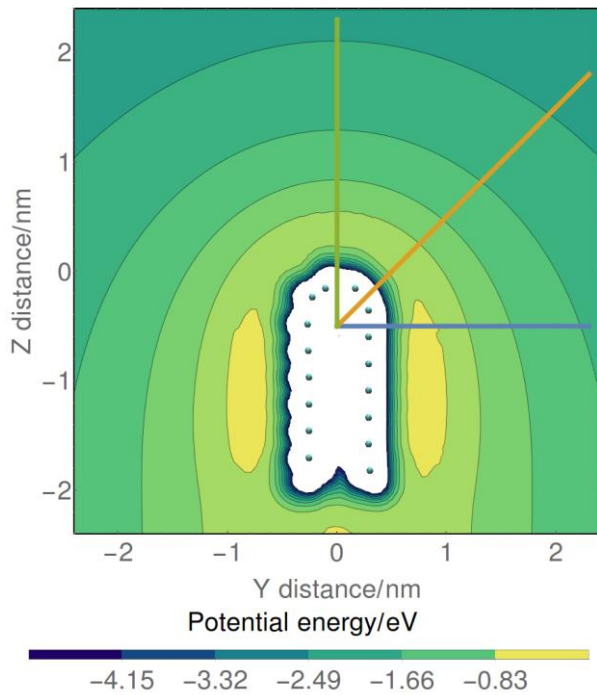


Fig. 7. Section containing the CNT axis, showing the potential distribution around the CNT tip with a background field of 0.08 Vnm^{-1} . The coloured lines indicate the directions (green = 0° , orange = 45° and blue = 90° relative to the axis) used for the potential plots of Fig. 8. The dots indicate the positions of carbon cores.

Fig. 8 shows the distribution with distance radially from a point on the axis near the centre of the hemispherical cap, for three angles relative to the axis and three values of applied field. When a field is applied with a suitable polarity to emit electrons, then at distances greater than about 0.5 nm from a core the potential is lowered, as expected. A more surprising effect that can also be seen is that at smaller radii, close to a core, increasing the field *raises* the potential. This happens for all three directions shown and implies that negative charge is being added near the cores. However, this should be expected since the unbound charge is free to move to terminate the increased field.

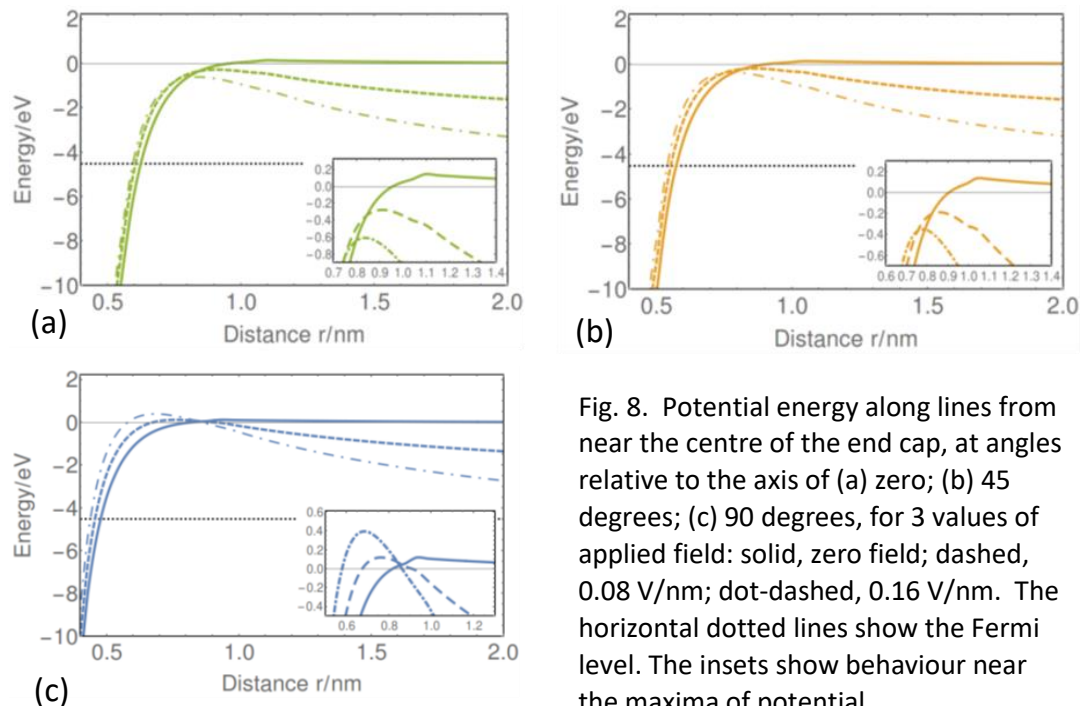


Fig. 8. Potential energy along lines from near the centre of the end cap, at angles relative to the axis of (a) zero; (b) 45° degrees; (c) 90° degrees, for 3 values of applied field: solid, zero field; dashed, 0.08 V/nm ; dot-dashed, 0.16 V/nm . The horizontal dotted lines show the Fermi level. The insets show behaviour near the maxima of potential.

The application of an anode-cathode voltage of 8V has two effects on the density of states. One is that the distribution of DoS with energy, while retaining substantially the same profile, moves to a range of energy lower by about 0.65 eV. The second is that the Fermi level rises by 0.64eV (relative to vacuum level), which is reasonable since the application of field induces more charge into the system. Application of the field causes the HOMO to be a higher orbital than in zero field.

4. Discussion

The detailed modelling of this short CNT section at atomic scale shows many differences of behaviour from the classical approximations that have been used hitherto. Much of the electron density is localised around the carbon cores, but there is also a continuous sheath of low electron density (as in the left-hand images of Fig. 2) that allows conduction over all the CNT surface.

One observation concerns the electron density outside the cores, forming the surface distribution of charge. This surface electronic charge forms a dipole layer with the carbon cores at the surface and creates a potential difference that is a major contribution to the work function of the CNT. Figures 2 and 6 show that the density in zero field is much larger than the change of density induced by an external field. Since the charge distribution is little affected by applied field, we expect also the potential difference between cores and vacuum level to be almost independent of the applied field (but the difference between Fermi level and vacuum may vary with field).

When an external field is applied with polarity to aid emission, the potential falls as distance from the mesh defined by the cores exceeds a certain value (Fig. 8). This lower limit, of about 0.5nm for the current geometry, is called here the screening distance. Fig. 8 also shows that at smaller spacings from the surface containing the cores, the potential *increases* with external field and the local field remains at a high value, typically many times the field applied for field emission (and of opposite polarity). This strong field within the screening distance is clearly influenced more by the dipolar charge than by the applied field. Thus the influence of static charge dominates over a range extending from the the cores to a surface separated from them by the screening distance.

It has long been recognised that the field is unlikely to change by an abrupt step from zero to an externally-applied value near the emitting 'surface' [1]. The most widely-used alternative assumption [9], [10] has been obtained from the expected image force on an electron near an ideally continuous, conducting plane. A concept that is more in agreement with atomic structure might be the force on an electron due to nearby partly-screened cores. However, it is desirable to include also the effect of all the background charge in the screening region. This is of course the calculation that has now been done by the DFT method in producing the potential solution of Fig. 8. Hence ~~it is suggested that~~ the exchange-and-correlation contribution to the DFT solution, ~~which is self-consistent for all charge around the CNT,~~ is a more accurate guide to the potential near the emitters than the image potential for any single electron.

When two conductors are electrically connected, their Fermi levels align. If a voltage difference is maintained between them, this difference appears between the Fermi levels. Thus for a fully-conducting CNT connected to a cathode plane, with a voltage V_{ak} between anode and cathode, we can say that the Fermi levels of anode and CNT differ by eV_{ak} . In the DFT calculation, however, the cathode plane is far away and the Fermi level of the CNT section is not automatically kept constant when a field is applied. For the calculations discussed here, we assume that the CNT is electrically

connected to a cathode potential that is defined as zero. Thus for discussion of DoS with different applied fields, we take the Fermi level as fixed. With this assumption, the effect of applying a field to aid emission is to lower the energy range of the DoS profile, relative to the Fermi level. This increases the number of states below the Fermi level, so providing states for the extra electrons induced by the field.

The number of orbitals calculated by ONETEP corresponds to the number of electrons in the system. Hence the number of orbitals to be expected for the full length of the CNT is far more than are in the short section reported here. This raises a question about how the distribution of states would change with the length of the CNT, which is currently being investigated. That said, the smaller number of orbitals reported here is enough to provide a graphical estimate of the Fermi level at 1000 K. At lower temperatures, the mid-gap value can be used as an estimate.

The spatial distribution of the HOMO for zero field, reported above, appears to have a maximum on the axis. If emission was mainly from this region, this could explain the observed limited divergence of field-emitted electrons. However, the maximum HOMO amplitude on the axis is inside the core cage, so may be shielded from the applied field; also, the result above is for a (5,5) SWCNT, and other emitters may behave differently.

As indicated in the Method section above, compatibility between the classical and atomic models requires agreement as to what outline in the atomic model should be taken as 'the surface' for the classical calculation. Since the classical surface of a conductor is an equipotential, it is obviously desirable to relate it to an equipotential in the atomic model. A potential difference between classical conductors corresponds to the same difference between their Fermi levels, so there is a case for taking the equipotential at the Fermi level to define the outline of the classical equivalent. This should produce an accurate potential distribution over the DFT box for use in the DFT calculation, and the barrier region starts directly at the surface thus defined. However, part of the screening region is outside the Fermi equipotential, and therefore the charge associated with this outer region lies outside the surface defined in this way.

5. Conclusions

Use of the DFT program ONETEP with boundary conditions set by classical modelling has given much more detail of the atomic properties of a capped CNT than is available from classical approximations. Among other outputs, it provides (a) estimates of the Fermi level (and work function) of the hemispherical cap at non-zero temperatures, (b) the spatial distribution of individual orbitals including the HOMO, and (c) distribution of the potential step at the surface, ~~which is a desirable replacement for the image potential~~. All these quantities are important for the estimation of field-emitted current.

The calculations also suggest that electronic charge extends further between the carbon cores and the barrier region than would be expected from known screening theory. An external field typical of field emission has little effect on the strong core-directed field within this screening region.

The DFT calculation provides estimates of occupancy near the Fermi level that can be used straightforwardly to estimate the work function of the surface.

The spatial distribution of the HOMO in general differs from that of the charge distribution. The HOMO for the analysed SWCNT appears to have a maximum on the axis, unlike the charge density.

Acknowledgments

The authors thank Prof. M.C. Payne, Prof. C-K. Skylaris and many members of the TCM Group, C.U. Department of Physics, for the suggestion of using ONETEP and their advice in running it.

Declarations of interest: none.

The research leading to these results has received funding from the People Programme (Marie Curie Actions) of the European Union's Seventh Framework ProgrammeFP7/2007-2013/ under REA grant agreement n 606988.

References

- [1] R.H. Fowler, L. Nordheim, Electron Emission in Intense Electric Fields, *Proc. R. Soc. London Ser. A-Mathematical Phys. Sci.* 119 (1928) 173–181. doi:10.1098/rspa.1928.0091.
- [2] D.A. Zanin, H. Cabrera, L.G. De Pietro, M. Pikulski, M. Goldmann, U. Ramsperger, D. Pescia, J.P. Xanthakis, Fundamental Aspects of Near-Field Emission Scanning Electron Microscopy, in: *Adv. Imaging Electron Phys.* Vol 170, 2012: p. 227.
- [3] X. Zheng, G.H. Chen, Z. Li, S. Deng, N. Xu, Quantum-Mechanical Investigation of Field-Emission Mechanism of a Micrometer-Long Single-Walled Carbon Nanotube, *Phys. Rev. Lett.* 92 (2004) 12–15. doi:10.1103/PhysRevLett.92.106803.
- [4] G. Csányi, C.-K. Skylaris, A. Nevidomskyy, C.J. Edgcombe, Ab initio approach to a lightning rod, Electronic Structure Discussion Group Seminar, TCM Group, Cambridge, 30 November 2005, <http://www.tcm.phy.cam.ac.uk/~nnd21/esdg.html>.
- [5] Z. Li, Density functional theory for field emission from carbon nano-structures, *Ultramicroscopy.* 159 (2015) 162–172. doi:10.1016/j.ultramic.2015.02.012.
- [6] C.-K. Skylaris, P.D. Haynes, A.A. Mostofi, M.C. Payne, Introducing ONETEP: Linear-scaling density functional simulations on parallel computers, *J Chem Phys.* 122 (2005) 084119. doi:10.1063/1.1839852.
- [7] J. Schneider, J. Hamaekers, S. Chill, S. Smidstrup, J. Bulin, R. Thesen, A. Blom, K. Stokbro, ATK-ForceField: a new generation molecular dynamics software package, *Model. Simul. Mater. Sci. Eng.* 25 (2017) 085007. doi:10.1088/1361-651X/aa8ff0.
- [8] FlexPDE, <http://www.pdesolutions.com>.
- [9] L. Nordheim, The effect of the image force on the emission and reflexion of electrons by metals, *Proc. R. Soc. London Ser. A-Mathematical Phys. Sci.* 121 (1928) 626.
- [10] R.E. Burgess, H. Kroemer, J.M. Houston, Corrected Values of Fowler-Nordheim Functions $v(y)$ and $s(y)$, *Phys. Rev.* 90 (1953) 515.